




ARTICLE

DOI: 10.1038/s41467-018-04377-4

OPEN

Dlx1/2 and Otp coordinate the production of hypothalamic GHRH- and AgRP-neurons

Bora Lee¹, Janghyun Kim², Taekyeong An³, Sangsoo Kim³, Esha M. Patel⁴, Jacob Raber^{4,5}, Soo-Kyung Lee ^{2,6}, Seunghee Lee ⁷ & Jae W. Lee ²

Despite critical roles of the hypothalamic arcuate neurons in controlling the growth and energy homeostasis, the gene regulatory network directing their development remains unclear. Here we report that the transcription factors Dlx1/2 and Otp coordinate the balanced generation of the two functionally related neurons in the hypothalamic arcuate nucleus, GHRH-neurons promoting the growth and AgRP-neurons controlling the feeding and energy expenditure. *Dlx1/2*-deficient mice show a loss-of-GHRH-neurons and an increase of AgRP-neurons, and consistently develop dwarfism and consume less energy. These results indicate that Dlx1/2 are crucial for specifying the GHRH-neuronal identity and, simultaneously, for suppressing AgRP-neuronal fate. We further show that Otp is required for the generation of AgRP-neurons and that Dlx1/2 repress the expression of Otp by directly binding the *Otp* gene. Together, our study demonstrates that the identity of GHRH- and AgRP-neurons is synchronously specified and segregated by the Dlx1/2-Otp gene regulatory axis.

¹Center for Neuroscience, Korea Institute of Science and Technology (KIST), Seoul 02792, Korea. ²Neuroscience Section, Papé Family Pediatrics Research Center, Department of Pediatrics, Oregon Health and Science University, Portland, OR 97239, USA. ³Department of Bioinformatics and Life Science, Soongsil University, Seoul 06978, Korea. ⁴Department of Behavioral Neuroscience, Oregon Health and Science University, Portland, OR 97239, USA. ⁵Departments of Neurology and Radiation Medicine, and Division of Neuroscience, Oregon National Primate Research Center, Oregon Health and Science University, Portland, OR 97239, USA. ⁶Vollum Institute, Oregon Health and Science University, Portland, OR 97239, USA. ⁷College of Pharmacy and Research Institute of Pharmaceutical Sciences, Seoul National University, Seoul 08826, Korea. Correspondence and requests for materials should be addressed to S.L. (email: leeseung@snu.ac.kr) or to J.W.L. (email: leejw@ohsu.edu)

The hypothalamus is a central regulator of the homeostatic processes that are essential to survival and reproduction^{1,2}. Among the multiple hypothalamic nuclei, the arcuate nucleus (ARC) is particularly receptive to various peripheral cues because it is located in proximity to the blood stream. Thus, in the central nervous system, the ARC serves as a primary gatekeeper and processor for the peripheral signals in directing the growth, energy balance, and reproductive behaviors in response to such cues^{1,2}. Numerous investigations for the past decades^{1,2} significantly enhanced our understanding of physiological roles of the ARC. The highly interconnected actions among the arcuate neurons in striking the body homeostasis raise the possibility that the distinct arcuate neuronal types are generated in a coordinated manner during hypothalamus development. However, the gene regulatory network that orchestrates their production remains poorly understood.

The ARC is composed of many different types of neurons that express specific sets of neuropeptides and elicit disparate physiological actions³. These include the agouti-related protein (AgRP)-neurons and pro-opiomelanocortin (POMC)-neurons, which play crucial roles in maintaining energy homeostasis¹. The AgRP-neurons secrete AgRP and neuropeptide Y (NPY), both of which increase food intake and decrease energy expenditure. In contrast, the POMC-neurons express both cocaine and amphetamine-related transcript (CART) and melanocyte-stimulating hormone- α (α MSH), which is derived from the precursor peptide POMC. The α MSH released from POMC-neurons decreases food intake and increases energy expenditure¹. Thus, the AgRP- and POMC-neurons exhibit the opposing activities in determining the levels of food intake and energy consumption. Interestingly, 17–25% of AgRP-neurons are derived from POMC-expressing cells⁴, indicating a close developmental link between AgRP- and POMC-neurons. Another critical neuronal type in the ARC is the growth hormone-releasing hormone (GHRH)-neurons that release GHRH². The GHRH triggers the secretion of the growth hormone (GH) from the anterior pituitary gland². GH then triggers expression in the liver of insulin-like growth factor 1 (IGF1). IGF1 regulates bone epiphyses, growth plate development, muscle and adipose tissue development, and glucose homeostasis². The control for nutritional status and linear growth needs to be coupled. Supporting this notion, it has been well-established that GH/GHRH levels are inversely correlated with the circulating level of the anorexic hormone leptin that targets arcuate neurons to control the energy balance^{5–7}. Given the physiological importance of the tight linkage between the energy balance and linear growth, it is possible that the production of GHRH-neurons is coordinated with the generation of AgRP- and/or POMC-neurons. To date, however, little has been known about whether and how the development of growth-promoting GHRH-neurons is connected to the formation of AgRP- or POMC-neurons that regulate the energy homeostasis.

Distal-less homeobox-1 (Dlx1) and its homolog Dlx2 are the homeodomain transcription factors that play important and redundant roles in the fate specification of GABA⁺ and tyrosine hydroxylase (TH)⁺ neurons in the forebrain^{8–12}. The immunohistochemical analyses with a pan-Dlx antibody detecting multiple Dlx factors revealed that Dlx factors are expressed in TH⁺ neurons and non-AgRP-neuronal type GABA⁺ neurons in the ARC¹³. Adult Dlx1-null mice show a twofold reduction in the number of TH⁺ neurons in the ARC¹³; whereas, the role of Dlx2 in the hypothalamus remains unexplored. We found that Dlx1 and Dlx2 are robustly expressed in the embryonic ARC by analyzing the three datasets, www.brain-map.org, www.genepaint.org, and the seminal work of Blackshaw and colleagues¹⁴, consistent with the earlier report¹⁵. This expression pattern suggests a possible role of Dlx1 and Dlx2 in the fate specification or differentiation of

arcuate neurons. Orthopedia (Otp) is the homeodomain transcription factor that is expressed in the several hypothalamic nuclei including the ARC¹⁶. Otp-null mice die perinatally and lack somatostatin (Sst)⁺ arcuate neurons¹⁶, suggesting a role of Otp in the ARC development. Interestingly, Otp and Dlx1 are expressed in alternating domains in the embryonic hypothalamus^{16–18}, and Dlx1 expression domain is expanded in presumptive paraventricular nuclei (PVN) in Otp-null mice¹⁶, suggesting an antagonistic relationship between the two transcription factors. However, the role of Dlx1/2 and Otp in the fate specification of arcuate neurons and how Dlx1/2 and Otp are linked in the gene regulatory network that governs the production of distinct arcuate neuronal types remains poorly understood.

Here our studies revealed that Dlx1/2 and Otp are required for the specification of GHRH- and AgRP-neurons, respectively. Furthermore, we found that Dlx1/2 suppress AgRP-neuronal fate by directly binding and repressing the *Otp* gene, uncovering a novel Dlx1/2-Otp gene regulatory axis critical for the segregation of GHRH- and AgRP-neuronal fates. Together, our data provide, for the first time, the evidence that GHRH- and AgRP-neuronal fates are interconnected, and suggest that the Dlx1/2-Otp axis plays a role in producing a balanced ratio of AgRP- to GHRH-neurons in the hypothalamus.

Results

Dlx1/2 are expressed in the developing ARC. To understand the role of Dlx1 and Dlx2 in ARC development, we investigated their expression pattern in the developing murine hypothalamus. We found that both Dlx1 and Dlx2 are highly enriched in the ARC at E16.5 (Fig. 1a). Consistently, the publically available datasets (www.brain-map.org, www.genepaint.org and Shimogori et al.¹⁴) show that Dlx1 and Dlx2 are highly expressed in the mediobasal hypothalamus, from which the ARC is derived, at E11.5, and that Dlx1/2 continue to be expressed in the ARC in the mature brain. These overlapping expression patterns suggest that Dlx1 and Dlx2 may function redundantly in the ARC, similarly to their roles in the developing forebrain¹¹.

We next analyzed the expression of Dlx1 in GHRH-, AgRP-, and POMC-neurons, the three major types of ARC neurons that control the growth and energy balance. In the embryonic ARC, Dlx1 was expressed in most GHRH-neurons (Fig. 1b), whereas it was not expressed in POMC-neurons that are visualized by the *Pomc-eGfp* transgenic allele¹⁹ (Fig. 1c). As AgRP expression in the ARC begins only perinatally, we labeled AgRP-neurons in the embryonic ARC using the *Npy-hrGfp* transgenic mice²⁰, in which GFP is expressed in embryonic AgRP-neurons before the induction of AgRP. At E14.5 and E17.5, Dlx1 was mostly excluded from GFP⁺ neurons (Fig. 1d), although 12–15% of GFP⁺ neurons that express GFP at a low level were co-stained with Dlx1 (arrows in Fig. 1d).

We also examined the expression of Dlx1 in other cell types in the ARC. Our results revealed that Dlx1 is expressed neither in KNDy-neurons (which express Kiss1) (Supplementary Fig. 1a, b) nor tanyctes in the ARC (Supplementary Fig. 1c). We also found that Dlx1 is expressed in neither Olig2⁺ oligodendrocytes nor GFAP⁺ astrocytes in the ARC (Supplementary Fig. 2a, b).

Taken together, these results suggest that Dlx1 may play a role in the development of GHRH-neurons, but less likely in the formation of POMC-neurons, AgRP-neurons or other arcuate cell types.

Dual roles of Dlx1/2 in GHRH-/AgRP-neuronal fate decision.

To inactivate both Dlx1 and Dlx2 in the developing ARC, we generated conditional Dlx1/2-null mice (*Dlx1/2^{cKO}*) in which the genomic region encompassing *Dlx1* and *Dlx2* genes is deleted by

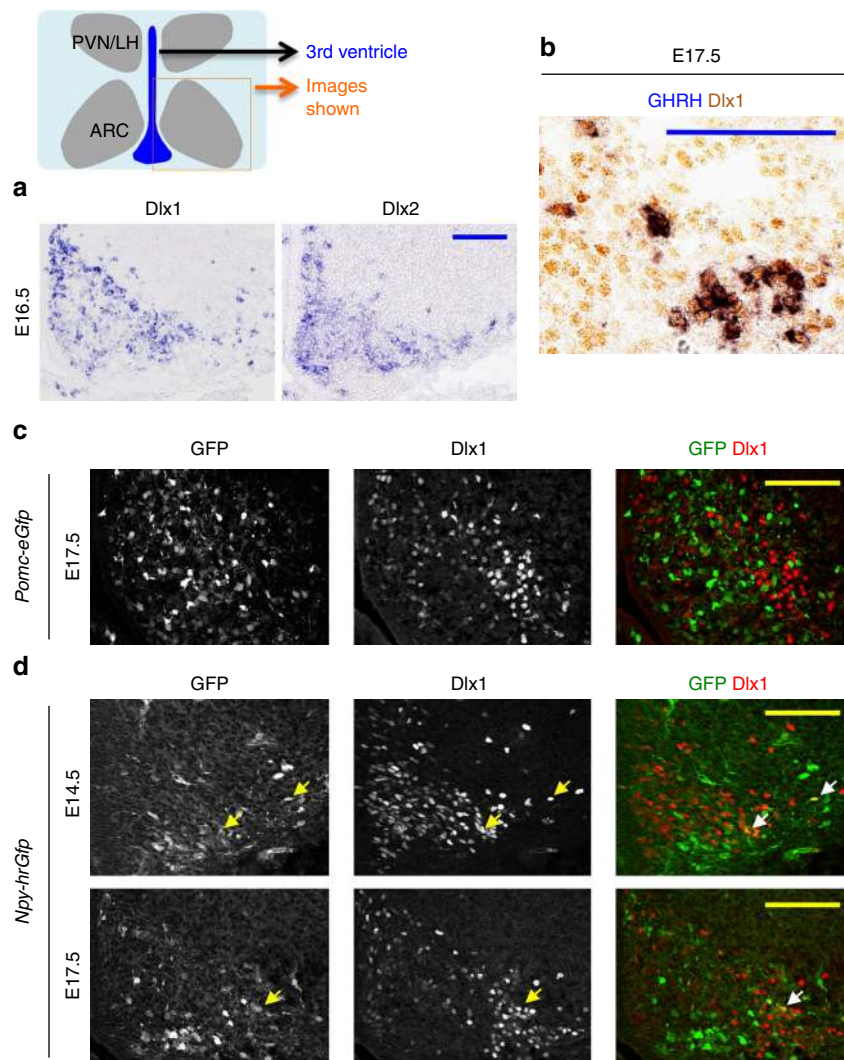


Fig. 1 Expression of Dlx1 in the developing ARC. **a, b** In situ hybridization (ISH) for Dlx1 and Dlx2 (**a**) and ISH for GHRH combined with immunohistochemistry (IHC) for Dlx1 (**b**). A total of $88.5 \pm 5\%$ of GHRH⁺ cells were Dlx1⁺ cells in IHC (**b**). **c, d** IHC analyses of Dlx1 expression in *Pomc-eGfp* (**c**) and *Npy-hrGfp* (**d**) embryos using our home-made antibodies against Dlx1. In *Pomc-eGfp*, none of GFP⁺ cells was Dlx1⁺ in IHC (**c**). In E14.5 *Npy-hrGfp*, $15 \pm 1\%$ of GFP⁺ cells were Dlx1⁺ in IHC, while $93 \pm 1\%$ of Dlx1⁺ cells did not express GFP (**d**). In E17.5 *Npy-hrGfp*, $12 \pm 2\%$ of GFP⁺ cells were Dlx1⁺ in IHC, while $90 \pm 3\%$ of Dlx1⁺ cells did not express GFP (**d**). Quantification was performed with multiple embryos and at least three sections from each embryo, and representative images for only one side of the ARC are as shown. Scale bars, 100 μ m

Nkx2.1-Cre, which broadly deletes genes in several cell types of the developing ARC (e.g., GABA⁺, NPY⁺, POMC⁺, TH⁺ neurons)^{21,22}. Our immunostaining analysis confirmed that Dlx1 expression was eliminated in the ARC of *Dlx1/2^{cKO}* mice (Fig. 2a, Supplementary Fig. 3a). The overall shape of ARC was comparable between *Dlx1/2^{cKO}* embryos and their controls. Interestingly, the size of the ARC of *Dlx1/2^{cKO}* mice became smaller than their controls at postnatal stages, but the number of NeuN⁺ neurons were not different (Supplementary Fig. 3b), suggesting that the ARC of *Dlx1/2^{cKO}* mice may have a non-neuronal issue such as a decrease in extracellular matrix. Importantly, GHRH-neurons were lost in the ARC of *Dlx1/2^{cKO}* mice at E15.5 and P28 (Fig. 2b, c). TH⁺ neurons were also significantly reduced in the ARC of *Dlx1/2^{cKO}* mice (Fig. 2a). Given that $\sim 76\%$ of GHRH-neurons express TH²³, a loss-of-GHRH-neurons in *Dlx1/2^{cKO}* mice likely contributes to the reduction of TH⁺ neurons. In addition, the expression of *Gsx1* and *Hmx2*, which drive the expression of GHRH and *Gsx1*, respectively^{24,25}, was significantly reduced in E15.5 *Dlx1/2^{cKO}* ARC in comparison to their controls (Supplementary Fig. 3c). These results indicate that Dlx1/2 are required

for the production of GHRH-neurons during hypothalamus development.

Next, we asked whether the removal of Dlx1/2 affects other ARC neuronal types. Strikingly, we observed a marked increase in NPY expression in the ARC of *Dlx1/2^{cKO}* mice at E15.5 (Fig. 2b). Although it was difficult to count the exact number of NPY⁺ cells, more cells were labeled with NPY in *Dlx1/2^{cKO}* mice (Fig. 2b). These results raise an interesting possibility that the generation of AgRP-neurons increase in the absence of Dlx1/2. Consistent with this idea, the number of neurons expressing *Bsx1*, the transcription factor critical for AgRP gene induction²⁶, was also increased in the ARC of *Dlx1/2^{cKO}* mice (Fig. 2a). Also more cells (as determined by enhanced ISH signal density as well as a larger area of ISH signals) appear to be labeled with *Sst* in the ARC of *Dlx1/2^{cKO}* mice (Fig. 2b). Considering that a subtype of AgRP-neurons express *Sst*³, increased *Sst*⁺ neurons together with the increase in the number of *Bsx*⁺ neurons (Fig. 2a) can be, at least partly, attributed to an increase in the number of AgRP-neurons. In the postnatal hypothalamus, similar observations were also made for NPY and AgRP in *Dlx1/2^{cKO}* mice (Fig. 2c).

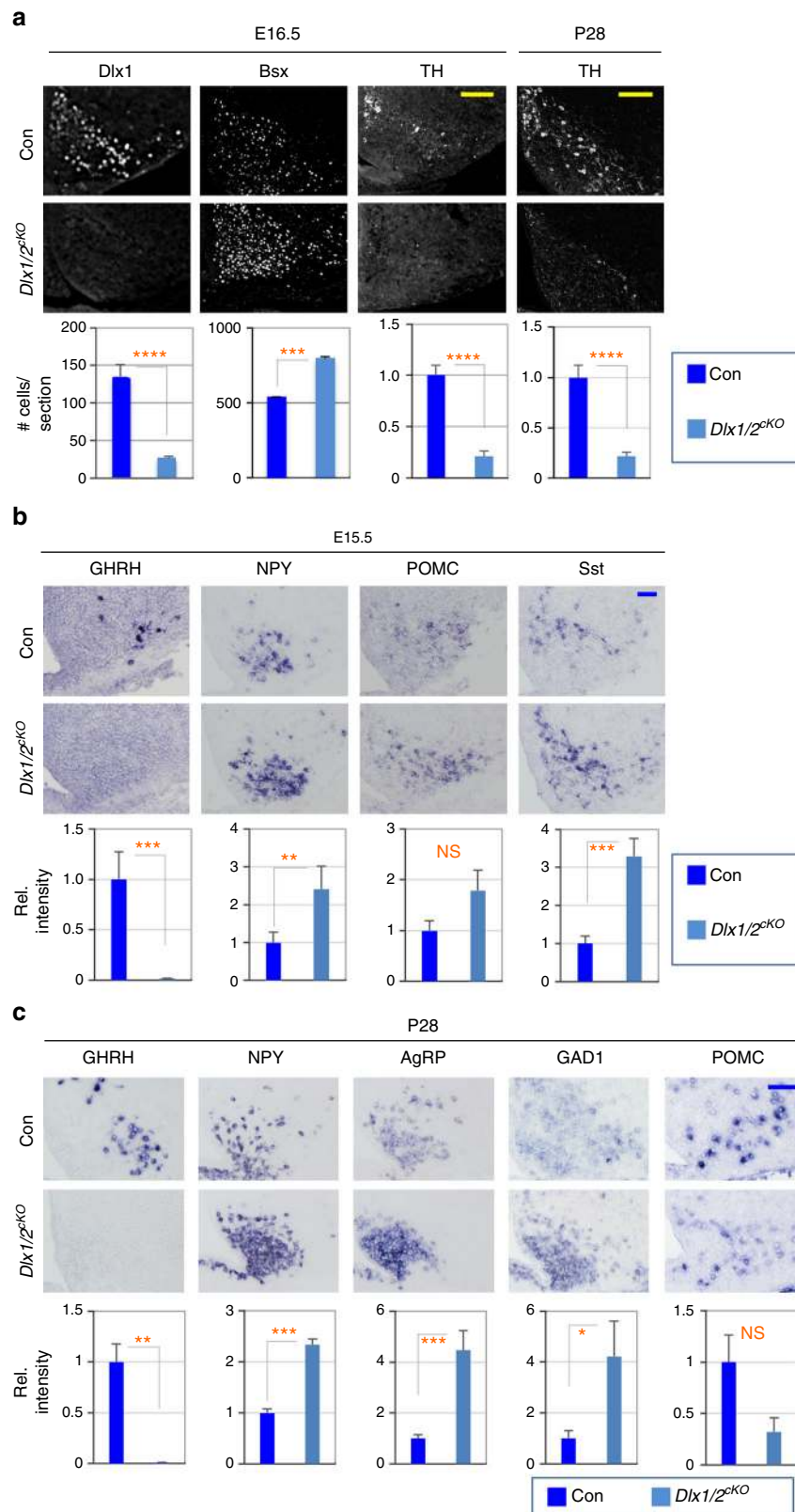


Fig. 2 Expression of arcuate neuropeptides in *Dlx1/2^{CKO}* mice. **a** IHC analyses of E16.5 *Dlx1/2^{CKO}* embryos ($n = 4$) revealed a significant decrease in the number of $Dlx1^+$ and TH^+ cells but a significant increase in the number of Bsx^+ cells relative to their littermate controls ($n = 4$). Similar observations were made for TH in the ARC of P28 *Dlx1/2^{CKO}* mice ($n = 3$) relative to their littermate controls ($n = 3$). **b** ISH analyses of *Dlx1/2^{CKO}* embryos ($n = 4$) revealed abolished expression of GHRH but a significant increase in the expression of NPY and Sst relative to their littermate controls ($n = 4$). **c** In ISH analyses, P28 *Dlx1/2^{CKO}* mice ($n = 3$) showed a significant increase in the expression of NPY, AgRP and GAD1 while losing the expressing of GHRH in comparison to their control mice ($n = 3$). The expression of POMC was not significantly altered (**b, c**). Quantification was performed with multiple embryos as indicated and at least 3 sections from each embryo, and representative images for only one side of the ARC are as shown. Scale bars, 100 μ m. Statistical differences were determined by Student's *t*-test: * $p < 0.05$, ** $p < 0.01$, *** $p < 0.001$, and **** $p < 0.0001$. Bars represent mean, error bars indicate the SEM

Consistent with the report that most AgRP-neurons are GABAergic²⁷, we also observed an increased expression of glutamate decarboxylase 1 (GAD1), a GABAergic neuronal marker (Fig. 2c). In contrast to NPY/AgRP, POMC expression did not show a significant difference between *Dlx1/2^{CKO}* and control mice (Fig. 2b, c). Together, in the absence of *Dlx1/2*, the formation of AgRP-neurons is likely facilitated and, interestingly, these aberrantly generated AgRP-neurons persist at postnatal stages in *Dlx1/2^{CKO}* mice.

Our results also revealed that the expression of *Kiss1*, a marker for KNDy-neurons in the ARC, was not significantly altered in *Dlx1/2^{CKO}* mice (Supplementary Fig. 4a), consistent with the lack of *Dlx1* expression in KNDy-neurons (Supplementary Fig. 1a, b).

Taken together, our results suggest that *Dlx1/2* are needed for the generation of GHRH-neurons and the suppression of AgRP-neuronal fate in the developing ARC. Our data suggest that *Dlx1/2* play a role in striking a balance between the formation of GHRH- and AgRP-neurons.

Defects in growth and energy expenditure in *Dlx1/2*-null mice.

A remarkable change in GHRH- and AgRP-neurons in *Dlx1/2^{CKO}* mice prompted us to ask how this alteration in ARC neuronal composition affects the growth and energy balance in mutant mice. While *Dlx1/2^{CKO}* mice were born according to the Mendelian ratio, ~47% of male and ~85% of female *Dlx1/2^{CKO}* mice died within 3 months after birth (Fig. 3a), indicating that they are vulnerable to death. Notably, the surviving *Dlx1/2^{CKO}* mice were dwarf as evident from their shorter body length and smaller body weight than the littermate controls at P28 (Fig. 3b, c). To investigate the activity of 'hypothalamic GHRH → pituitary GH → hepatic IGF1' axis, we monitored the expression of IGF1 in the liver and blood glucose levels. *Dlx1/2^{CKO}* mice displayed a drastic decrease in hepatic IGF1, as well as significantly reduced blood glucose levels compared to their littermate controls (Fig. 3c). Our data suggest that the hypothalamic GHRH signaling is likely impaired in *Dlx1/2^{CKO}* mice.

The two major actions of AgRP-neurons are to increase food intake and to reduce energy expenditure¹. Thus we analyzed if *Dlx1/2^{CKO}* mice, which appear to possess more AgRP-neurons in the hypothalamus, show any changes in these aspects. Intriguingly, by 3~4 months of age, *Dlx1/2^{CKO}* mice became obese and displayed significantly higher fat mass than the littermate controls despite their smaller body weight (Fig. 3d). This accumulated fat mass in *Dlx1/2^{CKO}* mice were even more evident when the reduced body weight was taken into consideration (right panel in Fig. 3d). In contrast, the lean mass decreased in *Dlx1/2^{CKO}* mice compared to their control mice (Fig. 3d). This obesity phenotype, along with increased AgRP expression in the hypothalamus, suggests that *Dlx1/2^{CKO}* mice may take more food and/or consume less energy. However, *Dlx1/2^{CKO}* and their control mice did not significantly differ in food intake throughout the diurnal cycles (Fig. 3e), suggesting that the orexigenic aspect of AgRP-neuronal action was not augmented in *Dlx1/2^{CKO}* mice (see discussion). We next monitored the energy expenditure by measuring oxygen consumption and carbon dioxide production. *Dlx1/2^{CKO}* mice showed a significantly lower energy consumption than their littermate controls (Fig. 3f). These results suggest that the energy saving aspect of AgRP-neuronal action was enhanced in *Dlx1/2^{CKO}* mice and that this at least partly contributed to the obese phenotype. Two of the major mechanisms for AgRP neurons to suppress energy consumption is to block locomotor activity²⁸ and thermogenesis^{29–31}. Interestingly, *Dlx1/2^{CKO}* mice showed strikingly reduced overall activity (Fig. 3g). Moreover *Dlx1/2^{CKO}* mice became sicker and died even earlier when housed individually than when accommodated as a group, pointing to the

possibility that *Dlx1/2^{CKO}* mice are impaired in maintaining the core body temperature. Indeed, *Dlx1/2^{CKO}* female mice showed a significantly lower body temperature than their controls at room temperature, and *Dlx1/2^{CKO}* male mice also displayed a similar trend for lower body temperature without reaching statistical significance (Fig. 3h). Also, the body temperature of *Dlx1/2^{CKO}* female mice dropped more quickly than their controls upon the cold exposure (5 °C) (Supplementary Fig. 3d). When we measured the expression of *Ucp1*, the major thermogenic factor in the brown adipocytes, 60 min after the cold exposure, when the body temperature of *Dlx1/2^{CKO}* female mice was lowest (Supplementary Fig. 3d), *Ucp1* expression was significantly lower in *Dlx1/2^{CKO}* female mice relative to control female mice (Supplementary Fig. 3e). Moreover, under the same condition (60 min post cold exposure), brown adipocytes of *Dlx1/2^{CKO}* female mice showed hypertrophy in comparison to control female mice (Supplementary Fig. 3f). Together, *Dlx1/2^{CKO}* mice, which appear to possess an increased number of AgRP-neurons in the hypothalamus, showed suppressed energy consumption but not increased food intake.

Collectively, our analyses revealed that *Dlx1/2^{CKO}* mice exhibit physiological changes in growth and energy balance in agreement with a loss-of-GHRH-neurons and a gain-of-AgRP-neurons in the hypothalamus.

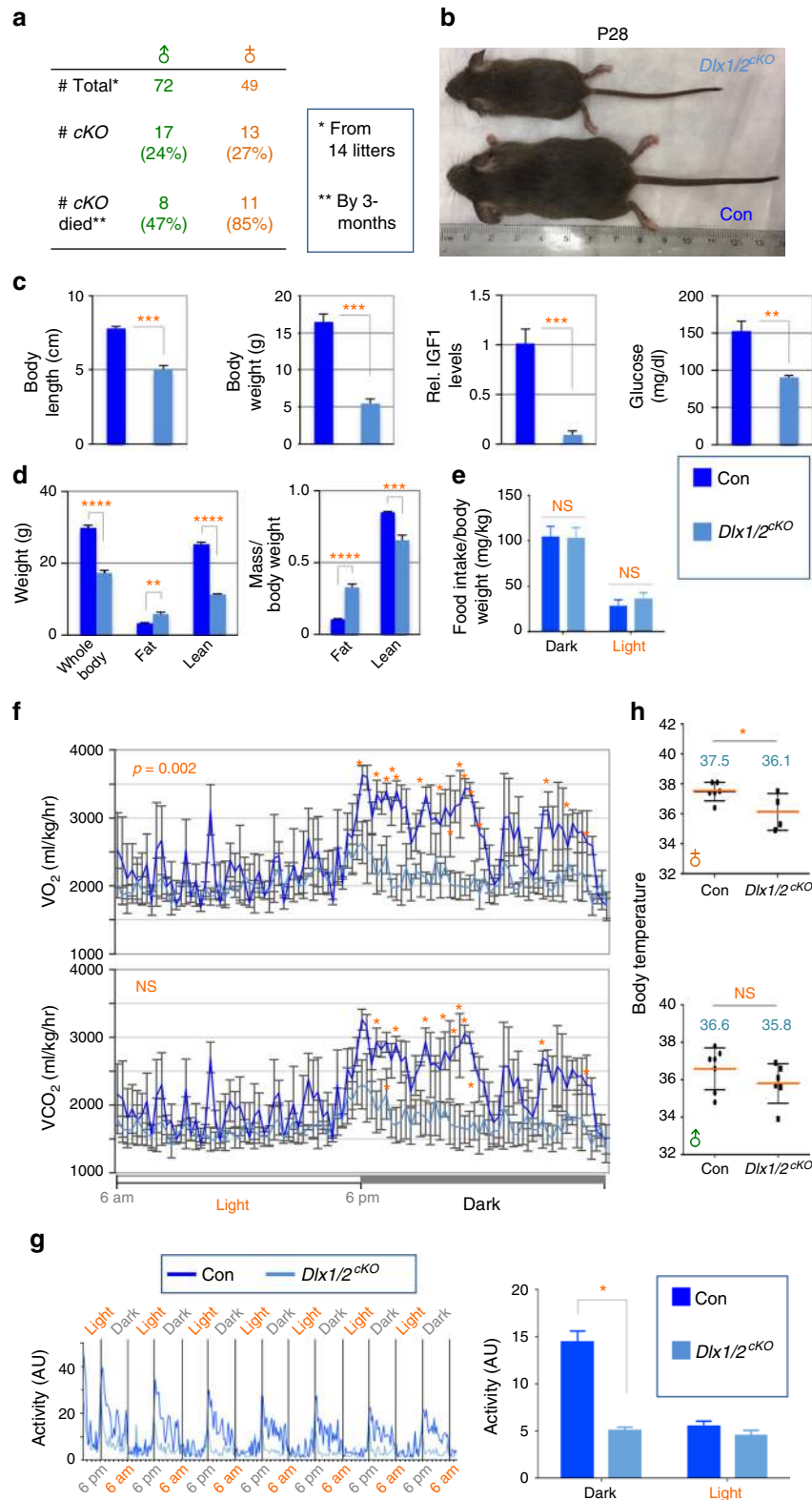
***Dlx1/2* directly bind and repress the *Otp* gene.** To elucidate the molecular mechanism by which *Dlx1/2* control the formation of GHRH- and AgRP-neurons in the developing hypothalamus, we performed ChIPseq analyses with our anti-*Dlx1* antibody (Supplementary Fig. 5) in E16 mouse hypothalami. We obtained a total of 932 *Dlx1*-bound ChIPseq peaks ($p < 0.001$), including a peak (P27) encompassing the previously reported *Dlx1/2*-bound binding site³² in the intergenic region of *Dlx5* and *Dlx6* (Supplementary Fig. 6a, Supplementary Data 1, GSE104372). Interestingly, ~80% of *Dlx1*-bound ChIPseq peaks were located in intergenic or intronic regions, whereas only ~11% of the peaks were found in the promoter region (Fig. 4a). De novo motif analysis revealed that two motifs are significantly enriched in *Dlx1*-bound genomic regions; *Dlx1/2*- and NHLH1-binding motifs (Fig. 4b). Both motifs were located around the summit of *Dlx1*-bound peaks (Fig. 4c), suggesting that they serve as the sequences recruiting *Dlx1* to the motif-bearing genomic regions.

Among putative direct target genes of *Dlx1* that our ChIPseq analyses identified, *Otp* is a good candidate for mediating the action of *Dlx1* in the ARC, given that *Otp* is expressed in the ARC and it is important for the formation of *Sst*⁺ neurons in this region¹⁶. *Dlx1* was recruited to a peak located at ~4 kb downstream region of *Otp*, named *Otp*-P29 (Fig. 4d). Our ChIP assays in E16.5 hypothalami further validated the binding of *Dlx1* to *Otp*-P29 (Fig. 4e). *Otp*-P29 contains multiple *Dlx1/2*-binding motifs that are evolutionarily conserved, but not NHLH1-binding motifs (Supplementary Fig. 6b). To test how *Dlx1/2* influence the transcriptional activity of *Otp*-P29, we constructed a luciferase reporter whose luciferase expression is directed by *Otp*-P29. We also generated another luciferase reporter containing the known *Dlx1*-binding site in the *Dlx5/6* intergenic region³² (*Dlx5/6*-P27, Supplementary Fig. 6a). *Dlx1* and *Dlx2* enhanced the transcriptional activity of *Dlx5/6*-P27 in luciferase assays in HEK293 cells; whereas, the DNA-binding-defective mutant form of *Dlx2* (*Dlx2*-QE, Supplementary Fig. 5a) failed to do so (Fig. 4f, Supplementary Fig. 7a), consistent with the report that *Dlx1/2* activate the expression of *Dlx5/6* by binding to *Dlx5/6*-P27 region³². In contrast to *Dlx5/6*-P27, *Dlx1* and *Dlx2* repressed the transcriptional activity of *Otp*-P29, whereas *Dlx2*-QE did not (Fig. 4f, Supplementary Fig. 7a), suggesting that *Dlx1/2* directly bind to

Dlx1/2-response elements and inhibit the transcriptional activity of *Otp*-P29. To further test the effect of Dlx1 on *Otp*-P29 in vivo, we generated a GFP reporter whose GFP expression is driven by *Otp*-P29, and electroporated this *Otp*-P29:GFP reporter with Dlx1 expression vector or control vector in chick neural tube using an *in ovo* electroporation technique. Dlx1 inhibited GFP expression driven by *Otp*-P29 in the neural tube (Fig. 4g), indicating that Dlx1 binding to *Otp*-P29 leads to transcriptional repression

in vivo (Fig. 4h). Interestingly, the ectopically expressed Dlx1 also suppressed the endogenous expression of *Otp*, but not that of *Isl1*, in the ventral neural tube (Supplementary Fig. 7b), further demonstrating that Dlx1 inhibits *Otp* expression in vivo.

To test the regulatory relationship between Dlx1/2 and *Otp* in the ARC, we examined their expression profile in the developing ARC. Dlx1 and *Otp* were expressed in a mutually exclusive pattern in the ARC of E13.5/14.5 WT mice (Fig. 4i). Interestingly,



Otp⁺ neurons markedly increased in the ARC of *Dlx1/2^{CKO}* mice at E13.5-P28 (Supplementary Fig. 3a, Fig. 4j), further supporting the idea that *Dlx1/2* suppresses Otp expression.

Taken together, our data demonstrate that *Dlx1/2* bind their binding sites located at ~4 kb downstream of the *Otp* gene and inhibit the expression of Otp in the developing ARC.

Otp is critical for the formation of AgRP-neurons. The identification of *Otp* as a downstream target gene of *Dlx1/2* in the hypothalamus led us to ask if Otp plays any role in the development of GHRH- and AgRP-neurons for which *Dlx1/2* play important roles. In the embryonic ARC of *Npy-hrGfp* mice, Otp was expressed in most GFP⁺ neurons (Fig. 5a, b). In contrast, most GHRH-neurons did not express Otp (Fig. 5c). We also found that KNDy-neurons, tanycytes, oligodendrocytes, astrocytes and TH⁺ neurons in the ARC do not express Otp (Supplementary Fig. 1a, c; Supplementary Fig. 2, a-c). These results suggest a role for Otp specifically in AgRP-neuronal development. Indeed, NPY⁺, AgRP⁺, and Sst⁺ neurons were entirely lost in the ARC of Otp-null mice at E16.5 and E18.5 (Fig. 5d, Supplementary Fig. 4b). Also *Gad1* ISH intensity was significantly reduced in Otp-null mice at P0 (Supplementary Fig. 4a), consistent with the loss-of-AgRP-neurons that are mostly GABAergic²⁷. These results suggest that Otp is required for the generation of AgRP-neurons. Consistently, the neurons that express GR and Bsx, the two transcription factors that are important for the expression of AgRP and NPY in the ARC^{26,33}, were greatly reduced in the Otp-deficient mice (Fig. 5e). In contrast, POMC⁺ and GHRH⁺ (as determined by ISH signal intensity) and TH⁺ neurons (as determined by the number of TH⁺ neurons) did not show a significant change in Otp-null ARC (Fig. 5d, e), suggesting that Otp is dispensable for the development of POMC- and GHRH-neurons. Consistent with the latter idea, the number of *Dlx1*⁺ neurons did not change significantly in Otp-null mice (Fig. 5e). These results also show that, in the developing ARC, Otp does not repress the expression of *Dlx1/2*, while *Dlx1/2* inhibits Otp expression. Interestingly, despite the lack of Otp expression in KNDy-neurons (Supplementary Fig. 1a), *Kiss1* expression was reduced in Otp-null mice at E18.5 (Supplementary Fig. 4a).

Taken together, our data highlight an essential role of Otp in directing the generation of AgRP-neurons.

***Dlx1/2* inhibits AgRP-neuronal fate via suppression of Otp.**

The increased Otp expression in *Dlx1/2^{CKO}* ARC, combined with the critical role of Otp in AgRP-neuron formation, begs the question of whether the de-repressed Otp in the absence of *Dlx1/2* drives the gain-of ectopic AgRP-neurons in *Dlx1/2^{CKO}* mice. If this is the case, the reduction of Otp levels in *Dlx1/2^{CKO}* mice will normalize AgRP-neuronal generation, but it will not restore GHRH-neuronal formation. To test this idea, we deleted a single copy of *Otp* in *Dlx1/2^{CKO}* mice (*Dlx1/2^{CKO};Otp^{+/-}*) and monitored the development of AgRP- and GHRH-neurons. Remarkably, the

aberrant gain-of AgRP-neurons in *Dlx1/2^{CKO}* mice was corrected when Otp levels were lowered in *Dlx1/2^{CKO};Otp^{+/-}* mice, but GHRH-neurons remained missing in *Dlx1/2^{CKO};Otp^{+/-}* mice (Fig. 6). These results establish that *Dlx1/2* suppress AgRP-neuronal fate by inhibiting Otp expression during ARC development.

Discussion

In this paper, we present a novel gene regulatory axis consisting of the homeodomain transcription factors *Dlx1/2* and Otp, which operates in the developing ARC. We propose that this *Dlx1/2*-Otp axis is critical for striking a balance between the embryonic generation of GHRH- and AgRP-neurons, and that this mechanism may contribute to a coordinate control of growth and energy homeostasis at postnatal stages (Fig. 7).

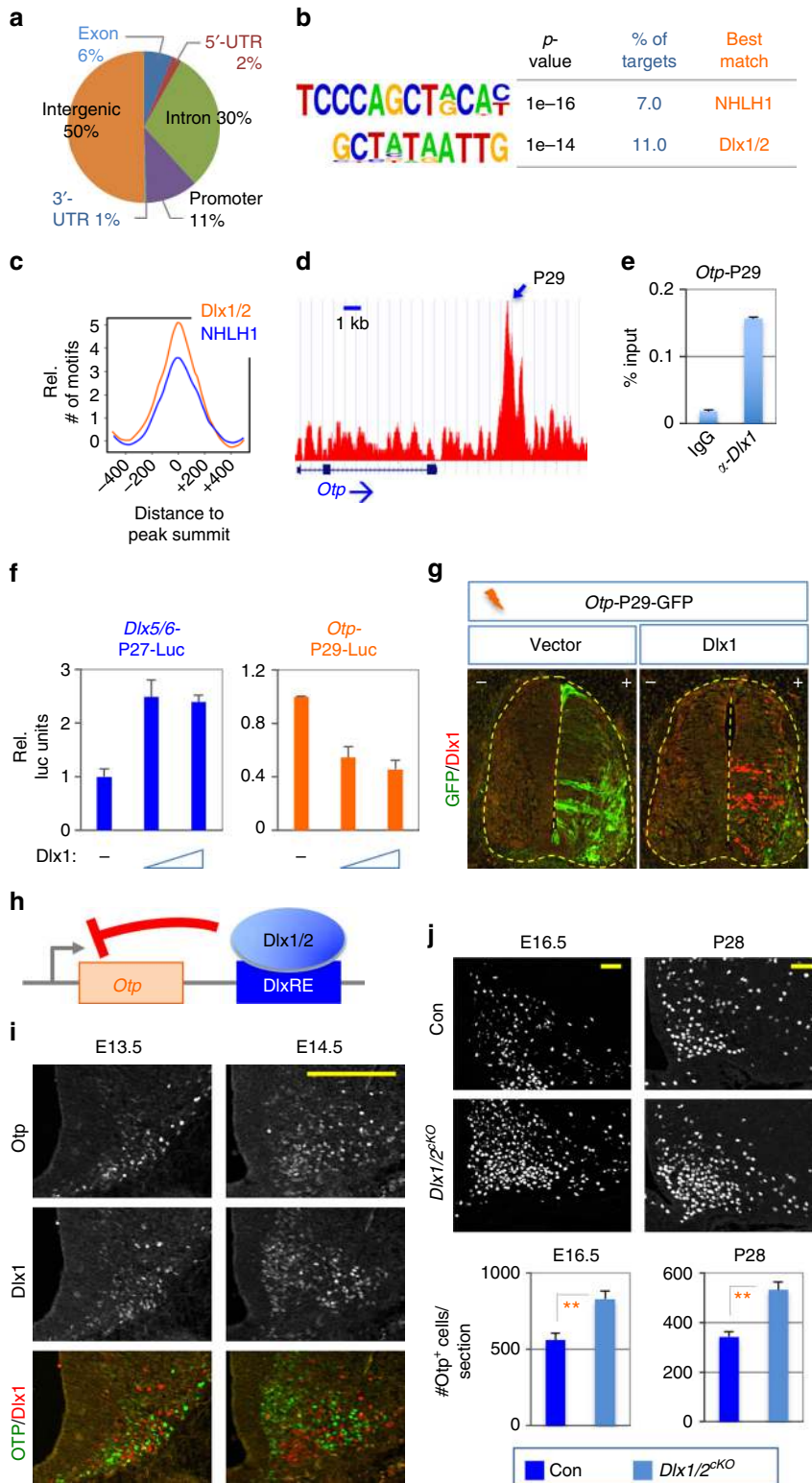
Given the interdependence between nutritional/energy status and linear growth⁵⁻⁷, it is possible that the development of energy homeostasis-controlling AgRP-/POMC-neurons and growth-promoting GHRH-neurons is synchronized, which may involve the differentiation of common precursors to related but distinct neuronal types. Our findings that the *Dlx1/2*-Otp gene regulatory axis is essential for the segregation of GHRH- and AgRP-neuronal fates indicate that the developmental pathways for GHRH- and AgRP-neurons are interconnected. In this regard, it is noteworthy that *Npy*-GFP⁺ cells can be divided into Otp⁺ and Otp⁻ populations. While a majority (~86%) of *Npy*-GFP⁺ cells express Otp in E14.5 ARC, ~14% of *Npy*-GFP⁺ cells do not (Fig. 5a). Interestingly, ~14% of *Npy*-GFP⁺ cells express *Dlx1* in E14.5 ARC (Fig. 1d). Combined with the finding that Otp and *Dlx1* expression is mutually exclusive in the embryonic ARC (Fig. 4i), these data raise the intriguing possibility that *Npy*-GFP⁺ population is composed of Otp⁺/*Dlx1*⁻ and Otp⁻/*Dlx1*⁺ cells, which give rise to AgRP- and GHRH-neurons, respectively. On a related note, in the developing ARC, POMC⁺ precursors generate several neuronal types, including POMC-, AgRP-, and fertility-regulating KNDy/*Kiss1*-neurons^{4,34}. Future investigation into the ontogeny of arcuate neurons, such as the relationship among POMC⁺ and *Npy*-GFP⁺ precursors and their progeny, will reveal how different types of arcuate neurons are produced in the right ratio during development to perform highly interconnected functions at postnatal stages.

Our data suggest that *Dlx1/2*-mediated repression of the *Otp* gene is the key to consolidating the GHRH-neuronal identity and keeping the number of AgRP-neurons in check. In *Dlx1/2*-null ARC, the number of Otp⁺ AgRP-neurons appeared to be increased at the expense of Otp⁻ GHRH-neurons (Figs. 2 and 4j; Supplementary Fig. 3a). Given the total number of neurons did not change significantly in *Dlx1/2*-null ARC (Supplementary Fig. 3b), the presumptive GHRH-neurons might have adopted AgRP-neuronal fate in the absence of *Dlx1/2*. It is also possible that, in addition to GHRH-neurons, some non-GHRH-neuronal types that normally express *Dlx1/2* (Fig. 1b) convert to AgRP-neurons in *Dlx1/2*-null ARC. The deletion of a single copy of the

Fig. 3 Growth and energy expenditure phenotypes of adult *Dlx1/2^{CKO}* mice. **a** Postnatal death of *Dlx1/2^{CKO}* mice from a total of 14 litters. **b, c** Dwarfism of *Dlx1/2^{CKO}* male mice ($n = 3$) (**b**) and qualification of their linear body length, body weight, IGF1 expression in the liver (by qRT-PCR) and serum glucose levels (**c**), relative to their littermate males controls ($n = 5$). The ruler unit in **b** is in cm. **d** MRI analyses of fat and lean mass revealed an increased fat deposition in *Dlx1/2^{CKO}* male mice ($n = 5$) relative to their control male mice ($n = 5$). **e** Food intake measurement revealed no significant difference between control ($n = 6$) and *Dlx1/2^{CKO}* male mice ($n = 4$) throughout the diurnal cycles. **f** VO_2/VCO_2 measurements uncovered a significant decrease in energy expenditure in *Dlx1/2^{CKO}* male mice ($n = 3$) relative to their controls ($n = 3$). **g** Circadian home cage activity was continuously measured using a home cage sensor system and mLog software (BioBServe, Germany). **h** Basal body temperature measurement revealed a significant reduction in female *Dlx1/2^{CKO}* mice ($n = 4$) relative to their littermate female controls ($n = 6$), as well as a trend for reduced body temperature with male *Dlx1/2^{CKO}* mice ($n = 6$) relative to their littermate male controls ($n = 6$), which did not reach statistical significance ($p, 0.06$). The p -values by two-way ANOVA test were 0.002 for VO_2 measurement but not significant (NS) for VCO_2 measurement, as indicated (**f**). Student's t -test results are as indicated: * $p < 0.05$, ** $p < 0.01$, *** $p < 0.001$, and **** $p < 0.0001$ (**c, d, f, h**). The home cage activity and food intake during the light and dark periods were analyzed separately using repeated-measures ANOVA with genotype as the between-subjects factor (**e, g**). Bars represent mean, error bars represent the SEM

Otp gene in *Dlx1/2*-null mice was sufficient to prevent the formation of ectopic AgRP-neurons (Fig. 6). Combined with a complete loss-of-AgRP-neurons in *Otp*-null mice (Fig. 5d), these results suggest that *Otp* plays an instructive role in AgRP-neuronal fate specification and that *Dlx1/2* inhibit the AgRP-neuronal fate mainly by repressing *Otp*, whose erroneous expression can divert the precursors to AgRP-neuronal fate. Notably, we and others have shown that *Dlx1* and *Otp* exhibit a

complementary expression pattern in multiple regions of the hypothalamus (Fig. 4i)^{16–18}, pointing to the possible cross-repressive interactions between *Dlx1* and *Otp*. Indeed, *Otp* was de-repressed in the ARC of *Dlx1/2*^{ckO} mice (Fig. 4j), but *Dlx1* expression did not alter in *Otp*-null ARC (Fig. 5e), indicating that *Dlx1/2* repress *Otp*, but not vice versa in the developing ARC. In contrast, in the PVN, the deletion of *Otp* resulted in the expansion of *Dlx1* expression domain¹⁶. Thus, different repressive



mechanisms may operate to generate the boundary between *Dlx1/2*- and *Otp*-expressing cells in a cell context-dependent manner.

AgRP-neurons are activated by food deprivation, and the stimulation of AgRP-neuronal circuitry promotes food intake and suppresses energy expenditure¹. The recent single-cell transcriptome analyses in the adult ARC revealed that AgRP-neurons are divided into the two molecularly distinct subtypes, *Sst*-expressing AgRP-neurons (*Sst*⁺AgRP⁺) and *Sst*-negative AgRP-neurons (*Gm8773*⁺AgRP⁺)³. However, it remains unclear if *Sst*⁺AgRP⁺ and *Gm8773*⁺AgRP⁺ subtypes play distinct roles in controlling energy balance and appetite. In light of the finding of AgRP-neuronal subtypes, it is noteworthy that an AgRP-neuronal subtype expressing *CRFR1* plays a regulatory role in adapting to cold stress²⁹. When this *CRFR1*⁺ AgRP-neuronal subtype was hyper-activated by the deletion of *CRFR1*, the female mutant mice showed lower body temperature with no change in food intake under basal conditions and dropped body temperature significantly more rapidly than control mice when exposed to 5 °C, but the male mutant mice did not show body temperature changes²⁹. These data suggest that *CRFR1*-expressing AgRP-neuronal subtype is involved in controlling body temperature, and needs to be inhibited to enable cold-induced thermogenesis. According to the gene expression profile studies in the adult ARC³, *CRFR1*⁺ AgRP-neurons are the *Sst*⁺AgRP⁺ subtype. Intriguingly, we found that *Dlx1/2*^{CKO} mice showed the increased levels of AgRP- and *Sst*-neurons in the ARC (Fig. 2). Similarly to the condition that hyper-activates *CRFR1*⁺ AgRP-neuronal subtype²⁹, *Dlx1/2*^{CKO} female mice exhibited significantly lower body temperature and were more susceptible to the cold stress than control mice without a change in food intake (Fig. 3e, h; Supplementary Fig. 3d), suggesting that the activity of *CRFR1*-expressing *Sst*⁺AgRP⁺ subtype is augmented in *Dlx1/2*^{CKO} mice. The increased cold-susceptibility in female *Dlx1/2*^{CKO} mice may be responsible, at least partly, for the higher death rate of female mice (Fig. 3a), particularly given that the standard temperature of our animal room (22 °C) could provide constant cold stress to mice^{35,36}. *Dlx1/2*^{CKO} mice also showed a reduced energy expenditure as monitored by oxygen consumption and carbon dioxide production (Fig. 3f), as well as a significantly decreased locomotor activity (Fig. 3g), both of which were likely reflected in a late-onset obesity (Fig. 3d). Taken together, in *Dlx1/2*^{CKO} mice, only an AgRP-neuronal subtype suppressing the energy consumption, but not the subtype stimulating the feeding behavior, may have been selectively increased. Alternatively, it is also possible that both AgRP-neuronal subtypes were aberrantly gained in *Dlx1/2*^{CKO} mice, but only a specific subtype (i.e., *CRFR1*⁺/*Sst*⁺ AgRP-neurons) was able to form the functional neuronal circuitry. A better understanding of AgRP-neuronal subtypes at the molecular, connectivity, physiology, and functional levels will help resolve this issue. Yet another possibility for future investigation is a possibility of GHRH-neurons interplaying with AgRP-

neurons in food intake control. Although, GHRH-null mice showed enhanced food intake³⁷, it is possible that the entire loss-of-GHRH-neurons themselves (which could be the case with our *Dlx1/2*^{CKO} mice) may differently alter the feeding behavior, particularly given the inverse correlation between GH/GHRH levels and the circulating level of the anorexic hormone leptin⁵⁻⁷.

Our finding that *Dlx1/2*^{CKO} mice show dwarfism, an absence of GHRH-neurons, and dysregulated GH signaling (Fig. 3b, c) establish *Dlx1/2* as essential players in the gene network directing the development of GHRH-neurons. Notably, the deletion of *Otp* in *Dlx1/2*-null mice failed to recover GHRH-neurons although it rescued the aberrant gain-of AgRP-neurons (Fig. 6), indicating that the *Dlx1/2*-*Otp* axis is not involved in promoting the GHRH-neuronal fate. Instead, in driving GHRH-neuron development, *Dlx1/2* may act as an upstream activator of *Hmx2/3* and *Gsx1*^{24,25}, given the marked downregulation of *Hmx2* and *Gsx1* in *Dlx1/2*-null ARC (Supplementary Fig. 3c). *Hmx2/3* are needed for the expression of *Gsx1*²⁴, which directly binds and triggers the transcription of the *GHRH* gene²⁵. Together, these findings propose the gene regulatory cascade, *Dlx1/2*-*Hmx2/3*-*Gsx1*-GHRH, which promotes the GHRH-neuronal identity in the developing ARC. Considering our results that *Dlx1/2* can function as either transcriptional activator or transcriptional repressor depending on a gene context in the same cell type (Fig. 4f, Supplementary Fig. 7a), it is interesting to postulate that *Dlx1* triggers the *Dlx1/2*-*Hmx2/3*-*Gsx1*-GHRH cascade via its transcriptional activator function, while repressing *Otp* as a transcriptional repressor in segregating the fates for GHRH- and AgRP-neurons in the precursors (Fig. 7). The future investigation is needed to understand the molecular basis for the gene context-specific dual roles of *Dlx1/2*.

Methods

Animals. All mice were housed in a pathogen-free animal facility under a normal 12 h light, 12 h dark cycle with ad libitum access to normal chow and water, unless otherwise noted. All studies were approved by the Institutional Animal Care and Use Committee of Oregon Health and Science University. *Npy-hrGfp* (#006417), *Pomc-eGfp* (#009593) and *Nkx2-Cre* (#008661) mice were purchased from the Jackson Laboratory. *Otp*^{+/-} and *Dlx1/2*^{fl} mice were kindly provided by Dr. Dario Acampora and Dr. Magdalena Petryniak, respectively.

Body temperature measurements. Anesthetized mice were implanted with Implantable Programmable Temperature and Identification Transponder (IPTT-300; Bio Medic Data Systems). Body temperature was measured using DAS-7009 reader (Bio Medic Data Systems).

Metabolic studies and food intake. Oxygen consumption and carbon dioxide production were measured using the indirect calorimetry system OxyMax (Columbus instruments). Data were collected after 72 h of acclimation with singly housed mice. Whole-body composition of 3–4-month-old mice were analyzed with EchoMRITM system. Intake of food was analyzed by weighing the amount of food in each cage at 6 am and 6 pm for two consecutive days. The mice were weighed on the second day and the food intake was analyzed per mouse and per g of body weight. For measuring locomotor activity, circadian home cage activity was continuously measured using a home cage sensor system and mLog software (BioServe, Germany). Mice were singly housed and given food and water ad libitum in

Fig. 4 Identification of *Otp* as a direct target gene of *Dlx1/2*. **a** Location of *Dlx1* ChIPseq peaks in the genome. **b, c** De novo motif analyses revealed that binding sites for two transcription factors, *NHLH1* and *Dlx1/2*, are enriched in our *Dlx1* ChIPseq peaks (**b**), which are mostly located in the summit area of *Dlx1* ChIPseq peaks (**c**). **d, e** Identification of *Dlx1* ChIPseq peak P29 associated with *Otp* (**d**) and validation of *Dlx1* binding to this peak in ChIP using anti-*Dlx1* antibody and E16.5 hypothalamic (**e**). Bars represent mean, error bars indicate the SD (**e**). **f** Luciferase assays in HEK293 cells, in which *Dlx1* activates the activity of *Dlx5/6*-P27-Luc reporter and represses the activity of *Otp*-P29-Luc reporter in a dose dependent manner (5 and 10 ng of *Dlx1* expression vector). Bars represent mean, error bars indicate the SD. The reporter assays were repeated four times, which produced similar results. A representative set of results is as shown. **g** *In vivo* expression of GFP by a reporter directed by P29 is strongly suppressed by coexpressed *Dlx1*. **h** Schematic model for *Dlx1/2* to suppress *Otp* expression via direct binding of *Otp*-*DlxRE* by *Dlx1/2*. **i** IHC analyses of *Otp*/*Dlx1* expression in E13.5 and E14.5 embryos using our home-made antibodies against *Otp* and *Dlx1*, in which *Dlx1* and *Otp* were expressed in a mutually exclusive pattern. **j** In IHC analyses, the number of *Otp*⁺ cells was significantly increased in *Dlx1/2*^{CKO} mice ($n = 4$ for E16.5, $n = 3$ for P28) relative to their littermate controls ($n = 4$ for E16.5, $n = 3$ for P28). In both stages, p -values in Student's t -test were <0.01 . Quantification was performed with multiple embryos as indicated and at least three sections from each embryo, and representative images for only one side of the ARC are as shown. Scale bars, 100 μ m. Bars represent mean, error bars represent the SEM

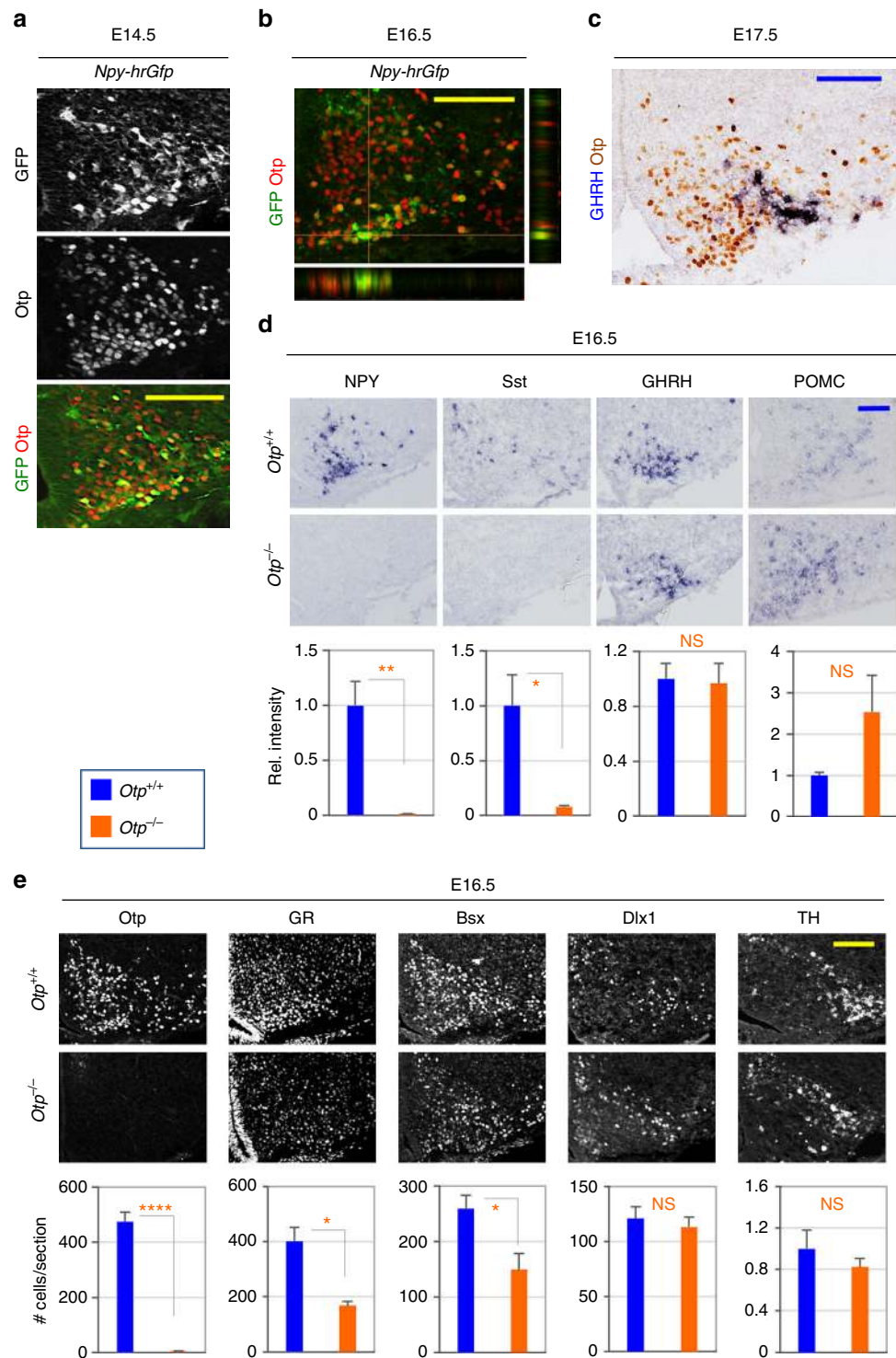


Fig. 5 Otp expression in AgRP-neurons and expression of arcuate neuropeptides in Otp-null embryos. **a** IHC analyses of Otp expression in *Npy-hrGfp* embryos using our home-made antibodies against Otp. $86 \pm 3\%$ of GFP⁺ cells were Otp⁺ cells in IHC. **b** A confocal Z-stack analysis was also performed with IHC analyses of Otp expression in E16.6 *Npy-hrGfp* embryos. **c** ISH for GHRH combined with IHC for Otp. $3 \pm 1\%$ of GHRH⁺ cells were Otp⁺ cells in IHC. **d** ISH analyses of E16.5 Otp-null embryos ($n = 3$) revealed a significant decrease in the expression of NPY and Sst but neither GHRH nor POMC in comparison to their littermate controls ($n = 4$). **e** IHC analyses of E16.5 Otp-null embryos ($n = 4$) revealed a significant decrease in the number of Otp⁺, GR⁺, and Bsx⁺ cells but neither Dlx1⁺ or TH⁺ cells relative to their littermate controls ($n = 4$). Quantification was performed with multiple embryos as indicated and at least three sections from each embryo, and representative images for only one side of the ARC are as shown. Scale bars, 100 μ m. Student's *t*-test results are as indicated: * $p < 0.05$, ** $p < 0.01$, and **** $p < 0.0001$ (**d, e**). Bars represent mean, error bars represent the SEM

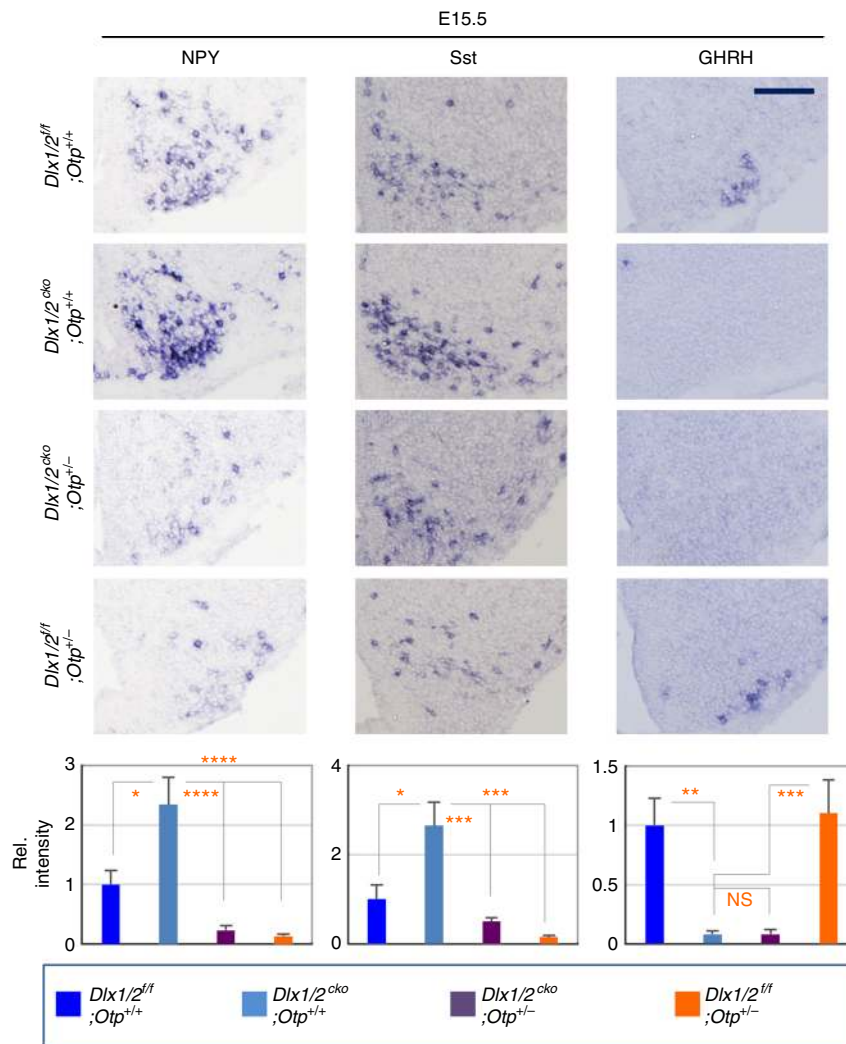


Fig. 6 *Dlx1/2* inhibits AgRP-neuronal fate via suppression of *Otp*. In ISH analyses, the expression of NPY and *Sst* in E15.5 $Dlx1/2^{cko};Otp^{+/-}$ embryos ($n = 5$) was significantly lower than that observed with their littermate $Dlx1/2^{cko};Otp^{+/+}$ embryos ($n = 3$) and rather comparable to that observed with $Dlx1/2^{fl};Otp^{+/+}$ ($n = 3$) and $Dlx1/2^{fl};Otp^{+/-}$ ($n = 11$) embryos. In contrast, the expression of GHRH was comparable between $Dlx1/2^{cko};Otp^{+/+}$ and $Dlx1/2^{cko};Otp^{+/-}$ embryos. Quantification was performed with multiple embryos as indicated and at least three sections from each embryo, and representative images for only one side of the ARC are as shown. Scale bars, 100 μ m. Student's *t*-test results are as indicated: * $p < 0.05$, ** $p < 0.01$, *** $p < 0.001$, and **** $p < 0.0001$. Bars represent mean, error bars represent the SEM

cages placed on a conventional Metro rack. Data were acquired every second and were averaged into 30 min bins for analysis.

Chick in ovo electroporation. The P29 ChIPseq peak region and *Dlx1* were subcloned into CMV-GFP reporter and RCAS expression vectors, respectively. Chicken eggs were incubated in a humidified chamber for 48–52 h. DNA constructs were injected into the lumen of chick embryonic spinal cord at HH stage 11–13. Electroporation was performed using a square wave electroporator (BTX). Incubated chicks were collected and fixed in 4% paraformaldehyde 3 days after electroporation.

ChIP. E16/E16.5 WT mouse hypothalami were dissected out and homogenized before being cross-linked with 1% formaldehyde for 10 min at room temperature, followed by quenching with 125 mM glycine. The cells were washed in PBS, and lysed in cell lysis buffer (5 mM PIPES, pH 8, 85 mM KCl, 0.5% NP40) and nuclear lysis buffer (50 mM Tris-HCl, pH 8, 10 mM EDTA, 1% SDS, protease inhibitor), followed by sonication. Cell lysates were redissolved in dilution buffer (0.5% Triton X-100, 5 mM EDTA, 150 mM NaCl, 25 mM Tris-HCl, pH 7.5, 0.5% deoxycholate, 0.1% SDS, protease inhibitor cocktail) and incubated with IgG and protein A agarose beads for 1 h for immunoclearing. The supernatant, collected after quick spin-down, was immunoprecipitated by our home-made anti-*Dlx1* antibody or control IgG (Santa Cruz) overnight, followed by incubation with protein A agarose for 2 h at 4 °C. The beads were sequentially washed with RIPA (0.1% SDS, 1% NP40, 1 mM EDTA, 50 mM Tris-HCl, pH 8.0, 150 mM NaCl, 0.5% deoxycholate),

high salt buffer (same as RIPA except 500 mM NaCl) and LiCl buffer (0.25 M LiCl, 1% NP40, 0.5% deoxycholate, 1 mM EDTA, 150 mM Tris-HCl, pH 8.0) for 10 min at each step. The beads were subsequently washed with TE buffer (10 mM Tris-HCl, 1 mM EDTA) three times. The protein/chromatin complexes were eluted in elution buffer (1% SDS, 1 mM EDTA, 0.1 M NaHCO₃, 50 mM Tris-HCl, pH 8.0) and reverse cross-linked by incubating at 65 °C overnight, followed by incubation at 50 °C for <2 h with proteinase K. The DNA was extracted with phenol/chloroform, followed by ethanol precipitation and solubilization in water.

Immunohistochemistry and in situ hybridization. Anesthetized mice were perfused transcardially with PBS and then with 4% paraformaldehyde. Brains were removed and placed in 4% paraformaldehyde overnight, washed with PBS, and incubated with 30% sucrose. Embryos were fixed in 4% paraformaldehyde and incubated in 30% sucrose. Brain sections (12 μ m thick) were prepared with a cryostat and incubated with primary antibodies at 4 °C overnight and followed by 1–2 h incubation with fluorescence-conjugated secondary antibodies (1:500, Jackson Immuno Research). To cover the representative ARC areas, we used at least three sections that are located ~144–168 μ m from each other. For ISH, antisense RNA probes were labeled with digoxigenin-UTP (Roche Diagnostics) according to the manufacturer's protocol. Hybridization was performed at 68 °C overnight. Hybridized sections were washed in 4 \times SSC and 0.2 \times SSC solution, and incubated with anti-digoxigenin-AP antibody (11093274910, Roche Diagnostics; 1:4000) overnight. The sections were subjected to color reaction with NBP/BCIP. The VECTASTAIN Elite ABC Kit (PK-6101, Vector Labs) was used according to the manufacturer's instruction for immunohistochemistry assay following ISH. The

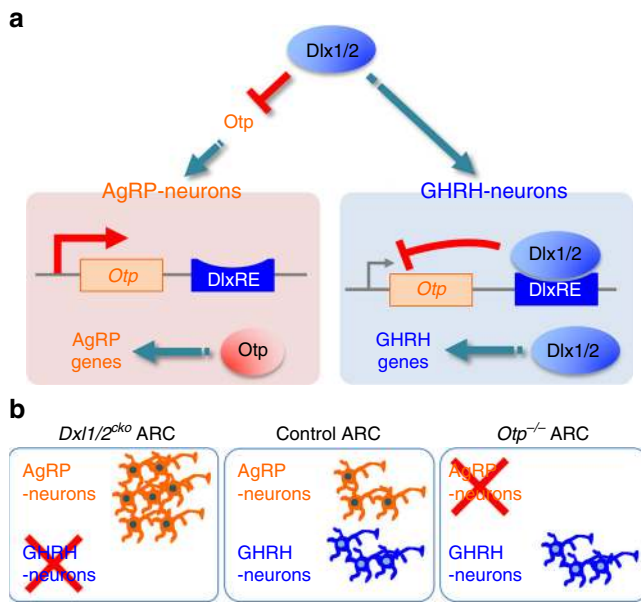


Fig. 7 Our working models. **a** A balanced production of AgRP- and GHRH-neurons is directed at least in part by the Dlx1/2-Otp gene regulatory axis, by which Dlx1/2 suppress Otp expression in developing GHRH-neurons. It remains to be determined if a similar gene regulatory axis that functions to block developing AgRP-neurons from adopting a GHRH-neuronal fate also exists. Also unclear is how Dlx1/2 and Otp control GHRH- and AgRP-neuronal genes, respectively. **b** Schematic representation of dysregulated production of AgRP- and GHRH-neurons in *Dlx1/2^{cko}* and *Otp^{-/-}* mice relative to control mice

probes for α MSH, AgRP, NPY, Sst, GHRH, Gad1, and Dlx1 were described previously³⁸. The antibodies used for immunohistochemistry are anti-GR (SC-1004, Santa Cruz; 1:500), anti-Isl1 (home-made; 1:3000), our home-made anti-Dlx1 (antibody), our home-made anti-OTP (using the 183–325 aa region of mouse Otp as the antigen), anti-Bsx³³ (1:2000), rabbit anti-NeuN (Ab177487, Abcam; 1:2000), rabbit anti-TH (AB152, Millipore; 1:500), and anti-GFP (GFP-1020, aves labs; 1:2000) antibodies.

Image analysis and quantification. A length of 12 μ m brain sections covering the entire arcuate nucleus were placed onto a series of slides with 4–5 sections on each slide. The distance between sections in single slide is 144–168 μ m. One slide from each mouse that contains matched sections was used to compare controls and mutants. Zeiss Axio imager 2 with apotome was used to image in situ hybridization and immunohistochemistry result. Integrated density measurement in Image J software was used to analyze densitometry. For cell counting, analyze particles measurement in image J was used to count specifically immuno-stained cells in the arcuate nucleus.

Co-immunoprecipitation and luciferase assay. Dlx1 and Dlx2 WT or Dlx2-QE mutant were subcloned into pcDNA3 plasmid with N-terminal triple Flag tag. ChIPseq peak P27 and P29 regions were cloned into TK-luciferase vector and used for luciferase assays. HEK293 cells were maintained in DMEM supplemented with 10% fetal bovine serum and penicillin/streptomycin. For co-immunoprecipitation assay, cells were seeded into 10 cm dishes and transiently transfected with either Dlx1 or Dlx2 expression vector using the standard calcium phosphate method. Anti-Flag M2 antibody (F3165, Sigma) was used for immunoprecipitation (1 μ g) and immunoblotting (1:3000), and a full size image with size markers is presented in supplementary Fig. 5. For luciferase assays, cells were seeded into 48-well plates and transiently transfected with luciferase reporter and Dlx1/2-expression vectors using SuperFect (Qiagen) according to the manufacturer's instruction. The actin- β -galactosidase plasmid was co-transfected for normalization of the luciferase results. Data are shown in relative luciferase units (mean \pm s.d.).

RNA extraction and quantitative RT-PCR analysis. Total RNAs were extracted from a piece of mouse liver using Trizol (Invitrogen) and reverse-transcribed using Thermo Scientific Maxima H Minus Reverse Transcriptase. The following primers were used with SYBR Green kit (Thermo Scientific Luminaris Color Hgreen, #K0371) for quantitative RT-PCR of IGf1: 5'-TCATGTCGTCTTCACACTCT-3' and 5'-TCCACAATGCTGTCTGAGG-3'.

Statistical analyses. Statistical differences were determined by Student's *t*-test. Statistical significance is displayed as follows: * $p < 0.05$, ** $p < 0.01$, *** $p < 0.001$, and **** $p < 0.0001$. The *p*-values for the CO_2/VO_2 measurements, as well as the body temperature measurement in the cold room were also analyzed using two-way ANOVA test. The home cage activity and food intake during the light and dark periods were analyzed separately using repeated-measures ANOVA with genotype as the between-subjects factor.

Data availability. Dlx1 ChIPseq data that support the findings of this study have been deposited in the National Center for Biotechnology Information Gene Expression Omnibus (GEO) and are accessible through the GEO Series accession number GSE104372. All other relevant data are available from the corresponding author on request.

Received: 29 November 2017 Accepted: 23 April 2018

Published online: 23 May 2018

References

- Hill, J. W., Elmquist, J. K. & Elias, C. F. Hypothalamic pathways linking energy balance and reproduction. *Am. J. Physiol. Endocrinol. Metab.* **294**, E827–E832 (2008).
- Bluet-Pajot, M. T. et al. Growth hormone secretagogues and hypothalamic networks. *Endocrine* **14**, 1–8 (2001).
- Campbell, J. N. et al. A molecular census of arcuate hypothalamus and median eminence cell types. *Nat. Neurosci.* **20**, 484–496 (2017).
- Padilla, S. L., Carmody, J. S. & Zeltser, L. M. Pomc-expressing progenitors give rise to antagonistic neuronal populations in hypothalamic feeding circuits. *Nat. Med.* **16**, 403–405 (2010).
- Considine, R. V. et al. Serum immunoreactive-leptin concentrations in normal-weight and obese humans. *N. Engl. J. Med.* **334**, 292–295 (1996).
- Dieguez, C. & Casanueva, F. F. Influence of metabolic substrates and obesity on growth hormone secretion. *Trends Endocrinol. Metab.* **6**, 55–59 (1995).
- Grinspoon, S. et al. Serum leptin levels in women with anorexia nervosa. *J. Clin. Endocrinol. Metab.* **81**, 3861–3863 (1996).
- Andrews, G. L., Yun, K., Rubenstein, J. L. & Mastick, G. S. Dlx transcription factors regulate differentiation of dopaminergic neurons of the ventral thalamus. *Mol. Cell Neurosci.* **23**, 107–120 (2003).
- Long, J. E. et al. Dlx-dependent and -independent regulation of olfactory bulb interneuron differentiation. *J. Neurosci.* **27**, 3230–3243 (2007).
- Cobos, I., Borello, U. & Rubenstein, J. L. Dlx transcription factors promote migration through repression of axon and dendrite growth. *Neuron* **54**, 873–888 (2007).
- Petryniak, M. A., Potter, G. B., Rowitch, D. H. & Rubenstein, J. L. Dlx1 and Dlx2 control neuronal versus oligodendroglial cell fate acquisition in the developing forebrain. *Neuron* **55**, 417–433 (2007).
- Qiu, M. et al. Null mutation of Dlx-2 results in abnormal morphogenesis of proximal first and second branchial arch derivatives and abnormal differentiation in the forebrain. *Genes Dev.* **9**, 2523–2538 (1995).
- Yee, C. L., Wang, Y., Anderson, S., Ekker, M. & Rubenstein, J. L. Arcuate nucleus expression of NKX2.1 and DLX and lineages expressing these transcription factors in neuropeptide Y(+), proopiomelanocortin(+), and tyrosine hydroxylase(+) neurons in neonatal and adult mice. *J. Comp. Neurol.* **517**, 37–50 (2009).
- Shimogori, T. et al. A genomic atlas of mouse hypothalamic development. *Nat. Neurosci.* **13**, 767–775 (2010).
- Eisenstat, D. D. et al. DLX-1, DLX-2, and DLX-5 expression define distinct stages of basal forebrain differentiation. *J. Comp. Neurol.* **414**, 217–237 (1999).
- Acampora, D. et al. Progressive impairment of developing neuroendocrine cell lineages in the hypothalamus of mice lacking the Orthopedia gene. *Genes Dev.* **13**, 2787–2800 (1999).
- Simeone, A. et al. Orthopedia, a novel homeobox-containing gene expressed in the developing CNS of both mouse and Drosophila. *Neuron* **13**, 83–101 (1994).
- Avantaggiato, V. et al. Developmental analysis of murine Promyelocyte Leukemia Zinc Finger (PLZF) gene expression: implications for the neuromeric model of the forebrain organization. *J. Neurosci.* **15**, 4927–4942 (1995).
- Cowley, M. A. et al. Leptin activates anorexigenic POMC neurons through a neural network in the arcuate nucleus. *Nature* **411**, 480–484 (2001).
- van den Pol, A. N. et al. Neuromedin B and gastrin-releasing peptide excite arcuate nucleus neuropeptide Y neurons in a novel transgenic mouse expressing strong Renilla green fluorescent protein in NPY neurons. *J. Neurosci.* **29**, 4622–4639 (2009).

21. Silbereis, J. C. et al. Olig1 function is required to repress *dlx1/2* and interneuron production in Mammalian brain. *Neuron* **81**, 574–587 (2014).
22. Xu, Q., Tam, M. & Anderson, S. A. Fate mapping *Nkx2.1*-lineage cells in the mouse telencephalon. *J. Comp. Neurol.* **506**, 16–29 (2008).
23. Phelps, C. J., Romero, M. I. & Hurley, D. L. Growth hormone-releasing hormone-producing and dopaminergic neurones in the mouse arcuate nucleus are independently regulated populations. *J. Neuroendocrinol.* **15**, 280–288 (2003).
24. Wang, W., Grimmer, J. F., Van De Water, T. R. & Lufkin, T. *Hmx2* and *Hmx3* homeobox genes direct development of the murine inner ear and hypothalamus and can be functionally replaced by *Drosophila Hmx*. *Dev. Cell.* **7**, 439–453 (2004).
25. Li, H., Zeitler, P. S., Valerius, M. T., Small, K. & Potter, S. S. *Gsh-1*, an orphan Hox gene, is required for normal pituitary development. *EMBO J.* **15**, 714–724 (1996).
26. Sakkou, M. et al. A role for brain-specific homeobox factor *Bsx* in the control of hyperphagia and locomotory behavior. *Cell Metab.* **5**, 450–463 (2007).
27. Horvath, T. L., Bechmann, I., Naftolin, F., Kalra, S. P. & Leranath, C. Heterogeneity in the neuropeptide *Y*-containing neurons of the rat arcuate nucleus: GABAergic and non-GABAergic subpopulations. *Brain Res.* **756**, 283–286 (1997).
28. Mesaros, A. et al. Activation of *Stat3* signaling in *AgRP* neurons promotes locomotor activity. *Cell Metab.* **7**, 236–248 (2008).
29. Kuperman, Y. et al. *CRFR1* in *AgRP* neurons modulates sympathetic nervous system activity to adapt to cold stress and fasting. *Cell Metab.* **23**, 1185–1199 (2016).
30. Ruan, H. B. et al. *O-GlcNAc* transferase enables *AgRP* neurons to suppress browning of white fat. *Cell* **159**, 306–317 (2014).
31. Steculorum, S. M. et al. *AgRP* neurons control systemic insulin sensitivity via *myostatin* expression in brown adipose. *Tissue Cell* **165**, 125–138 (2016).
32. Zerucha, T. et al. A highly conserved enhancer in the *Dlx5/Dlx6* intergenic region is the site of cross-regulatory interactions between *Dlx* genes in the embryonic forebrain. *J. Neurosci.* **20**, 709–721 (2000).
33. Lee, B. et al. Brain-specific homeobox factor as a target selector for glucocorticoid receptor in energy balance. *Mol. Cell Biol.* **33**, 2650–2658 (2013).
34. Sanz, E. et al. Fertility-regulating *Kiss1* neurons arise from hypothalamic POMC-expressing progenitors. *J. Neurosci.* **35**, 5549–5556 (2015).
35. Kokolus, K. M. et al. Baseline tumor growth and immune control in laboratory mice are significantly influenced by subthermoneutral housing temperature. *Proc. Natl Acad. Sci. USA* **110**, 20176–20181 (2013).
36. Feldmann, H. M., Golozoubova, V., Cannon, B. & Nedergaard, J. *UCP1* ablation induces obesity and abolishes diet-induced thermogenesis in mice exempt from thermal stress by living at thermoneutrality. *Cell Metab.* **9**, 203–209 (2009).
37. Recinella, L. et al. Effects of isolated *GH* deficiency on adipose tissue, feeding and adipokines in mice. *Growth Horm. IGF Res.* **23**, 237–242 (2013).
38. Lee, B., Lee, S., Lee, S. K. & Lee, J. W. The LIM-homeobox transcription factor *Isl1* plays crucial roles in the development of multiple arcuate nucleus neurons. *Development* **143**, 3763–3773 (2016).

Acknowledgements

We thank Dr. Daniel Marks for critically reading this manuscript. We thank Dr. Shaun Morrison's lab for helping us with the body temperature measurement. We also thank Drs. Dario Acampora and Dr. Magdalena Petryniak for providing *Otp^{+/-}* and *Dlx1/2^{fl/fl}* mice, respectively. This research was supported by grants from the NIH/NINDS (R01 NS054941 to S.-K.L.) and NIH/NIDDK (R01 DK064678 to J.W.L.; R01 DK103661, to S.-K.L. and J.W.L.), the Korea Health Technology R&D Project through the Korea Health Industry Development Institute, funded by the Ministry of Health and Welfare, Republic of Korea (HI17C0447 to S.L.), and National Research Foundation of Korea (NRF-2012M3A9D1054705 to S.K.). This work was partially supported by the development account of Dr. Raber.

Author contributions

B.L. designed and performed most of the experimental work, analyzed data and wrote the manuscript. J.K. assisted with metabolic profiling experiments. T.A. and S.K. assisted with bioinformatics analyses of our ChIPseq results, S.L., S.-K.L. and J.W.L. coordinated the study, designed the experiments and wrote the manuscript. All of the authors approved the manuscript.

Additional information

Supplementary Information accompanies this paper at <https://doi.org/10.1038/s41467-018-04377-4>.

Competing interests: The authors declare no competing interests.

Reprints and permission information is available online at <http://npg.nature.com/reprintsandpermissions/>

Publisher's note: Springer Nature remains neutral with regard to jurisdictional claims in published maps and institutional affiliations.



Open Access This article is licensed under a Creative Commons Attribution 4.0 International License, which permits use, sharing, adaptation, distribution and reproduction in any medium or format, as long as you give appropriate credit to the original author(s) and the source, provide a link to the Creative Commons license, and indicate if changes were made. The images or other third party material in this article are included in the article's Creative Commons license, unless indicated otherwise in a credit line to the material. If material is not included in the article's Creative Commons license and your intended use is not permitted by statutory regulation or exceeds the permitted use, you will need to obtain permission directly from the copyright holder. To view a copy of this license, visit <http://creativecommons.org/licenses/by/4.0/>.

© The Author(s) 2018